

TripletUNet: Multi-Task U-Net with Online Voxel-Wise Learning for Precise CT Prostate Segmentation

Kelei He, Chunfeng Lian, Ehsan Adeli, Jing Huo, Yinghuan Shi, Yang Gao,
Bing Zhang, Junfeng Zhang, Dinggang Shen, *Fellow, IEEE*

Abstract—Fully convolutional networks (FCN), including U-Net and V-Net, are widely-used network architecture for semantic segmentation in recent studies. However, conventional FCNs are typically trained by the cross-entropy or dice loss, in which the relationships among voxels are neglected. This often results in non-smooth neighborhoods in the output segmentation map. This problem becomes more serious in CT prostate segmentation as CT images are usually of low tissue contrast. To address this problem, we propose a two-stage framework. The first stage quickly localizes the prostate region. Then, the second stage precisely segments the prostate by a multi-task FCN-based on the U-Net architecture. We introduce a novel online voxel-triplet learning module through metric learning and voxel feature embeddings in the multi-task network. The proposed network has two branches guided by two tasks: 1) a segmentation sub-network aiming to generate prostate segmentations, and 2) a triplet learning sub-network aiming to improve the quality of the learned feature space supervised by a mixed of triplet and pair-wise loss function. The triplet learning sub-network samples triplets from the inter-mediate heatmap. Unlike conventional deep triplet learning methods that generate triplets before the training phase, our proposed voxel-triplets are sampled in an online manner and operates in an end-to-end fashion via multi-task learning. To evaluate the proposed method, we implement comprehensive experiments on a CT image dataset consisting of 339 patients. The ablation studies show that our method can effectively learn more representative voxel-level features compared with the conventional FCN network. And the comparisons show that the proposed method outperforms the state-of-the-art methods by a large margin.

Index Terms—Prostate cancer, Sampling, Metric learning, Fully convolutional networks, Contrast learning, Triplet



1 INTRODUCTION

THIS Fully convolutional networks (FCNs) are state-of-the-art in pixel-to-pixel or voxel-to-voxel prediction tasks, e.g., segmentation [1], [2], [3], [4], [5], [6] and localization/detection [7], [8], [9], primarily because of the encoder-decoder architectures that gradually integrate local to global features. However, existing methods typically train FCNs by minimizing a loss that averaged over all independent pixel/voxel locations, i.e., cross-entropy [1], [3] or Dice [4] loss, without considering inter-pixel/voxel semantic correlations in the learned feature space. As a consequence, these FCNs usually suffer from two common limitations: 1) they can only generate rough heatmap (or probability map) for indicating object location, but cannot produce finer segmentation for precisely delineating object boundaries [10]; 2) they may generate incomplete segmentation with

unsmooth boundaries or small fragmented pieces. These limitations are even more serious for prostate segmentation in computed tomography (CT) images, as shown by a representative example in Fig. 1 (a), since 1) CT images are often of low soft-tissue contrast, and 2) prostates usually have very unclear boundaries and also large variations across patients (See Fig. 2).

Graph-based post processing is a straightforward strategy, which has been used widely to refine segmentations by FCNs. For example, [10], [11] adopted fully connected conditional random fields (CRF) to model inter-pixel/voxel relationships in an image, based on which more smooth segmentation is generated by minimizing an energy function initialized with the FCN outputs. The successes of these graph-based post-processing methods reveal the importance of explicitly modeling inter-pixel/voxel relationships in segmentation. However, since post processing is generally performed offline and does not have any influence on pixel/voxel-wise feature learning, two independent stages may lead to suboptimal segmentation results.

We assume that, *synergistically modeling inter-pixel/voxel relationships along network training* can learn much more discriminative feature space for end-to-end image segmentation, compared with the case of solely using the cross-entropy or dice loss followed by offline post-processing. Based on this assumption, a multi-task FCN (called *Triplet-FCN*) is proposed in this paper and applied to segmenting prostates from raw (high-dimensional) CT images. Fig. 3

- K. He and J. Zhang are with the Medical School of Nanjing University, Nanjing, P.R. China. J. Huo, Y. Shi, Y. Gao are with the State Key Laboratory for Novel Software Technology, Nanjing University, Nanjing, P. R. China. K. He, Y. Shi, Y. Gao and J. Zhang are also with the National Institute of Healthcare Data Science at Nanjing University, Nanjing, P. R. China. B. Zhang is with Department of Radiology, Nanjing Drum Tower Hospital, Nanjing University Medical School, P. R. China.
- C. Lian and D. Shen are with the Department of Radiology and BRIC, University of North Carolina, Chapel Hill, NC, USA. D. Shen is also with the Department of Brain and Cognitive Engineering, Korea University, Seoul, Republic of Korea. E. Adeli is with the Department of Psychiatry and Behavioral Sciences and the Department of Computer Science at Stanford University, CA, USA.

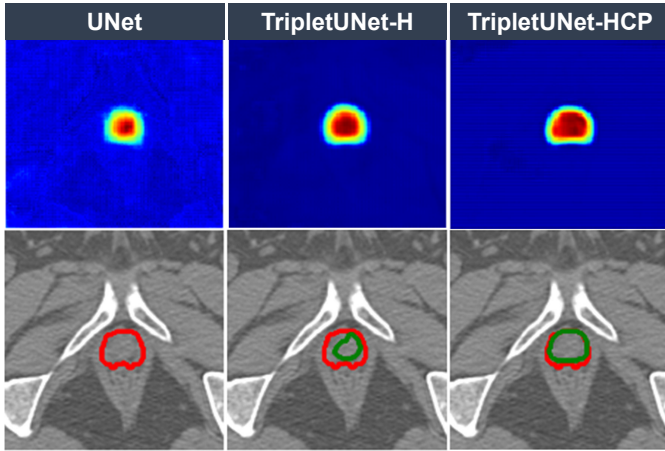


Fig. 1. Representative examples of heatmaps and respective segmentations produced by FCNs trained without versus with our proposed online voxel-triplet sampling (i.e., UNet versus TripletUNet-H and TripletUNet-HCP). UNet roughly identified prostate location but failed to delineate the prostate boundary. In contrast, our TripletUNet-H with the better learned voxel feature embeddings can generate segmentations in such challenging cases. Moreover, TripletUNet-HCP incorporates contour-aware mechanism can further delineate the fuzzy prostate boundary more precisely.

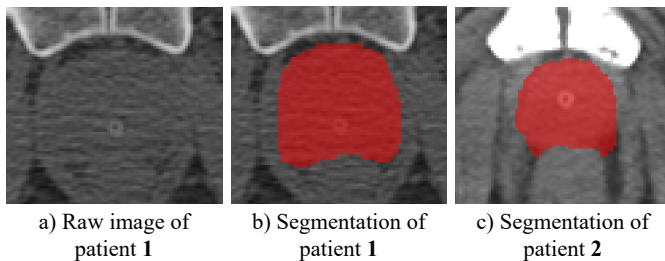


Fig. 2. A raw CT slice and the ground-truth prostate segmentations produced by an experienced radiologist for two typical patients. The fuzzy organ boundary is showed by a) and b), and the large inter-subject variation is showed by b) and c).

shows the schematic diagram of our method, with two major stages. Specifically, in Stage 1, we roughly locate prostate using a lightweight UNet trained with the down-sampled CT images. Then, in Stage 2, we crop each detected prostate region from the raw CT image for training our TripletFCN to obtain precise prostate delineation.

To improve voxel-level discriminative capacity of intermediate feature maps, we train TripletFCN by integrating *online voxel-triplet learning module* for concurrent metric learning. Notably, triplet metric learning had been previously used in image classification and retrieval tasks [12], [13] to learn representative image-level feature embedding, where semantically similar image pairs are pulled closer together while dissimilar ones are pushed further apart. By contrast, in this paper, we regard voxels in each CT image as individuals and then design three complementary sampling strategies (i.e., random, focal hard negative and contour-aware sampling) to generate voxel-triplets for the learning of segmentation-oriented voxel-level feature embedding. These design choices for our proposed voxel-triplet learning module leads to three main advantages:

- The sampled triplets can comprehensively model

inter-voxel relationships, thus driving the intermediate feature maps of the network to form a discriminative embedding space for more precise voxel-level classification, with an example shown in Fig. 1;

- Our triplet learning module is general and can be easily inserted into any existing architectures without the need for any additional learnable weights;
- It can be seamlessly cooperated with other modules. For example, in the task of CT prostate segmentation, our voxel-triplet learning module integrates contour-aware mechanism into triplet sampling, so as to more precisely delineate the prostate boundary.

We have evaluated our proposed method on a real patient CT image dataset consisting of 339 subjects, leading to superior performance compared with the state-of-the-art methods for image segmentation.

The rest of the paper is organized as follows. In Section 2, we introduce the related works for CT prostate segmentation and deep neural networks integrating the triplet-based learning. In Section 3, we introduce the proposed methods in detail. In Section 4, we extensively evaluate our proposed method. Finally, in Section 5, we conclude the proposed method and discuss the future work.

2 RELATED WORK

In this section, we review related work from two aspects: 1) existing automated methods developed for CT prostate segmentation, and 2) deep neural networks integrating triplet-based learning.

2.1 CT Prostate Segmentation

Most recent studies for CT prostate segmentation fall into two categories, i.e., deformable model-based or learning-based methods.

Deformable model-based methods typically initialize a mesh, which is then optimized to move towards the object surface. For example, Shao *et al.* [14] proposed a deformable model-based method which is jointly learned with a boundary regressor to include boundary information for guiding the prostate segmentation. Considering that mesh initialization is a common challenge for deformable-based methods, Gao *et al.* [15] proposed a context-based displacement regressor, which effectively eliminated bad initializations to improve the segmentation of male pelvic organs in CT images. However, these methods are affected by the initialization and the contrast of the organ boundary, that limited its performance.

In learning-based methods, a classifier is typically trained to identify the label of a voxel (e.g., background or prostate) with hand-crafted features or task-oriented features extracted by deep neural networks. For example, Shi *et al.* [16] proposed a method based on spatial-constrained transductive LASSO method to select couple feature representations, by assuming the low-level features are dependent. Shi *et al.* [17] proposed a multi-stage FCN-based segmentation method leveraging the ideology of domain adaption for CT prostate segmentation. Specifically, the manual delineation is fused with the image in different importance rate in each stage, and the fusion image is fed

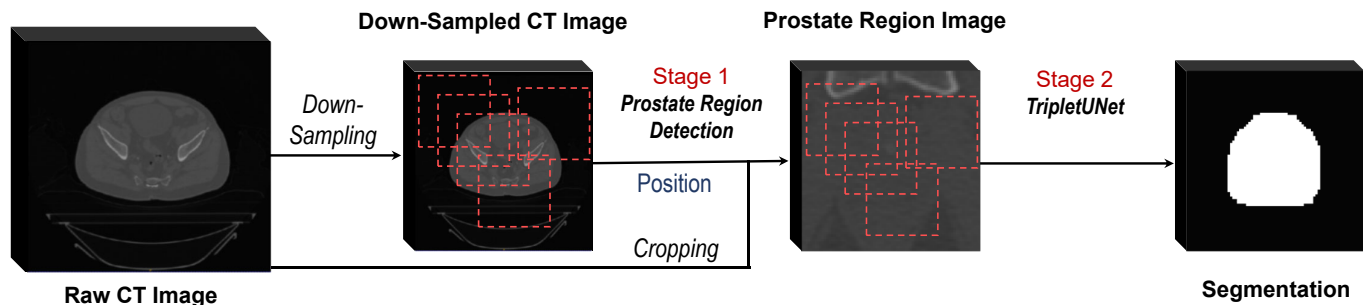


Fig. 3. The main stream of our proposed method. For simplicity, some complementary image processing procedures (e.g., body cropping, intensity and spatial normalization, training patch generation, etc.) are removed. The red dot boxes denote the random cropping strategy of the patches in training stage.

to the FCN in each stage for enhancing the appearance of the raw image. By taking the advantage of task-oriented learning and integration of local-to-global deep features, the FCN-based largely improves the performance of the prostate segmentation in CT images. However, the automated segmentations produced by these methods are often incomplete with imprecise prostate boundaries.

2.2 Triplet-based Deep Networks

Triplet loss is widely utilized with deep neural networks in classification and retrieval tasks, e.g., face recognition [13], [18], [19] and person Re-Identification (Re-ID) [12], [20]. Most applicable problems suffers from the large intra-class sample variations. The situation is similar to the case of medical image segmentation. For example, Schroff *et al.* [18] proposed a CNN-based method that integrates online sampling of triplet image patches to learn representative feature embedding for face recognition and clustering. Wang *et al.* [21] proposed to jointly learn from cross-image and single-image representations for person re-identification. Specifically, the network has three input branches to implement triplet-based learning.

However, all these existing methods perform triplet feature embedding at the image- or patch-level, i.e., there were not designed specifically for pixel-to-pixel prediction (e.g., segmentation). Notably, although a three-branch CNN was proposed in Lim *et al.* [22] to perform segmentation using multi-scale images, this method is also patch-based without explicit consideration of inter-pixel relationships. This motivated us to train a FCN with online voxel-triplet learning module to tackle the challenging task of CT prostate segmentation.

3 METHODS

Prostate is located in a relatively small area in the whole pelvic CT image. Precisely segmenting prostate directly from the raw CT image is practically challenging and computationally infeasible, considering that the noisy background can strongly mislead the network. Therefore, as the pipeline shown in Fig. 4, we design a two-stage deep learning framework to segmentation prostate in a coarse-to-fine fashion from raw CT images. Specifically, the first stage quickly detects the prostate while the second stage performs fine prostate delineation.

3.1 Prostate Detection

In the first stage, a detection network is utilized to locate the region of the prostate. Different from the conventional methods (e.g., the mass center [16]) which typically adopt statistical reference to roughly localize the prostate area, we follow our previous work [23] and use a lightweight UNet architecture to quickly and roughly segment the prostate on the down-sampled CT image.

Specifically, we down-sample the images into 1/4 size of the original scale by trilinear interpolation. Then, the network is trained with the 2D patches (size: $64 \times 64 \times 5$) randomly cropped from the down-sampled CT image in a sliding-window fashion. After training, we feed the whole down-sampled CT images into the trained UNet to obtain the coarse prostate segmentation. This strategy avoids voting for the patch-wise predictions. The prostate region is localized with this coarse prostate segmentation by roughly calculating the prostate centroid. Finally, we crop fixed-sized prostate region centered on the calculated centroid from the raw CT image, and use it as the input for fine prostate segmentation in the subsequent stage. In this work, the size of prostate region is set to $128 \times 128 \times 128$, which can cover the whole prostates for all training subjects.

3.2 Fine Prostate Segmentation

After getting the prostate region, in the second stage, we propose a multi-task FCN (i.e., denoted by TripletFCN-HCR) to generate fine prostate segmentation by introducing the online triplet learning mechanism.

3.2.1 Network Architecture

The architecture of an instantiation of our proposed TripletFCN, namely TripletUNet-HCR, is shown in Fig. 4. Similar to UNet [3], our TripletUNet-HCR is also an encoder-decoder architecture with skip connections for the extraction of voxel-level features that integrate local-to-global information. It consists of three down-sampling blocks, three up-sampling blocks, and an online voxel-triplet learning module with three complementary triplet sampling strategies. Specifically, TripletUNet-HCR has two sub-networks: 1) the segmentation sub-network for producing voxel-level predictions; 2) the voxel-triplet learning modules for modeling the inter-voxel relationships via voxel-level feature embedding. The detailed architecture of our TripletUNet-HCR is shown

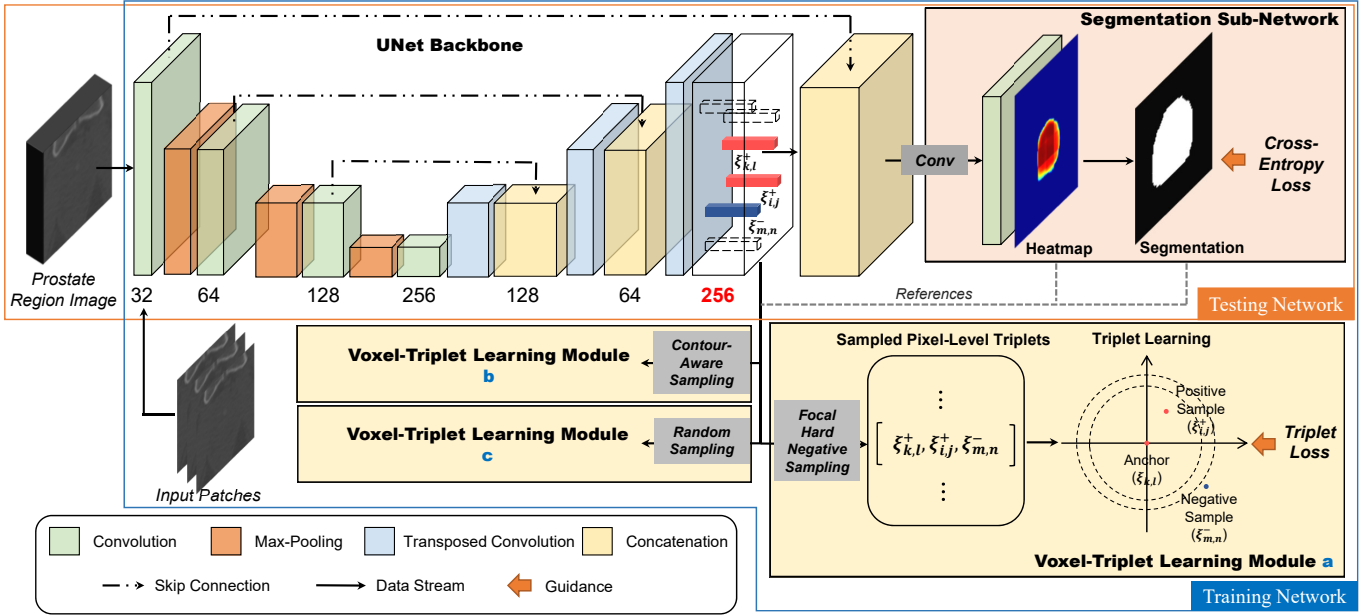


Fig. 4. The overall structure of the proposed TripletUNet-HCR (in Stage 2). The colored cubes denote the blocks with a specific operation layer (i.e., convolution, transposed convolution, pooling), and several complementary layers (e.g., convolutional layer, batch normalization layer, etc.). The details of the layers in different blocks are listed in Table 1. Please note that the segmentation sub-network and voxel-triplet learning modules in different network configurations are of similar structures.

in Table 1 comprising a total number of parameters of 3.28 million.

3.2.2 Voxel-Triplet Learning Module

As discussed earlier, conventional FCNs typically ignore the inter-voxel relationship in the learned deep feature space. Thus, they may lead to fragmented segmentation. To tackle this challenge, we propose a voxel-triplet learning module, by sampling online voxel-wise heatmaps to triplets.

In this case, each voxel (along with the respective voxel-level feature representation) is a candidate to generate the triplets. The operation is performed on the feature maps from the last convolutional layer of the last up-sampling block. Formally, given a mini-batch of N inputs, we denote the size of such feature maps as $N \times h \times w \times d$. Here, d denotes the feature length of the voxel. h, w denotes the feature height and width, respectively. As the voxel-level features may vary through each learning iteration, generating the whole set of triplets which has the quantities of $(N \times h \times w)^{(2 \times 3)}$ in each iteration is unacceptable. To effectively train the network, we select a subset of triplets in each iteration. Specifically, the selected triplets are first determined by k anchors, for which we randomly select m positive and negative samples.

As has been verified in previous work [18], [24], different sampling strategies may strongly affect the performance of the network. Therefore, in this work, we explore three sampling strategies, i.e., 1) random sampling, 2) focal hard negative triplet sampling, and 3) contour-aware triplet sampling, and combine them for our TripletFCN. A brief illustration of these three sampling strategies is shown in Fig. 5. In the experiments, the latter two triplet mining strategies are proven to help network achieve higher segmentation accuracy compared with the random sampling strategy.

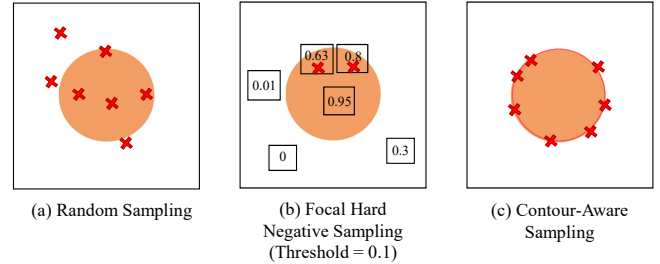


Fig. 5. A brief illustration of three different triplet sampling strategies. Red cross denotes the anchor point selected in one iteration. Please note that the box with value in (b) denotes the predicted probability of the point in a certain position. The orange round and circle denoted the reference ground-truth of segmentation of the prostate which indicates the positive labels in the triplet sampling scheme. The red circle in (c) denotes the prostate contour and used for selecting anchor candidates.

i) Random Triplet Sampling: A basic and intuitive sampling method to produce the triplets is the random sampling. In random sampling method, the anchors are randomly selected in the voxels which held the positive labels (see in Fig. 5 (a)). The positive and negative samples are then randomly selected accordingly.

ii) Focal Hard Negative Triplet Sampling: As proved by works in [12], [18], the random triplet sampling method may produce insufficient learned method, as the common triplets which satisfy the triplet distance assumption will dominate the training process. Therefore, these triplet embedding methods mine only the hard/semi-hard samples. The hard negative triplet mining strategy used in conventional methods is typically implemented by selecting the triplets, which have an {anchor,positive} pair with the maximum intra-class distance, and a {anchor,negative} pair with the minimum inter-class distance. Obviously, the

TABLE 1

Network architecture of the proposed TripletUNet-HCR. The 'Type' column lists the type of the layers, including, 'conv': convolutional layer; 'dconv': down-sampling with padding and matching convolutional layer; 'tconv': transposed convolutional layer; 'bn': batch normalization layer; 'r': ReLU layer; 'samp-h': focal hard negative triplet sampling; 'samp-c': contour-aware triplet sampling. 'Params' is formatted in {kernel size, stride, padding} for convolutional layers, {kernel size, stride} for pooling layers, and {kernel size, stride} for transposed convolutional layers. '#' denotes number of parameters.

Block	Layer Name	Type	Input	Params	#
conv block1	conv1a	conv+bn+r	image	3 × 3 × 32, 1, 1	0.9K
	conv1b	conv+bn+r	conv1a	3 × 3 × 32, 1, 1	9K
	pool1	max-pooling	conv1b	2, 2	-
conv block2	conv2a	conv+bn+r	pool1	3 × 3 × 64, 1, 1	18K
	conv2b	conv+bn+r	conv2a	3 × 3 × 64, 1, 1	37K
	pool2	max-pooling	conv2b	2, 2	-
conv block3	conv3a	conv+bn+r	pool2	3 × 3 × 128, 1, 1	74K
	conv3b	conv+bn+r	conv3a	3 × 3 × 128, 1, 1	147K
	pool3	max-pooling	conv3b	2, 2	-
conv block4	conv3a	conv+bn+r	pool2	3 × 3 × 256, 1, 1	295K
	conv3b	conv+bn+r	conv3a	3 × 3 × 256, 1, 1	590K
upblock1	upconv4a	tconv	dconv3	2, 2	131K
	concat4b	concat	upconv4a, conv3b	-	-
	conv4c	conv+bn+r	concat4b	3 × 3 × 128, 1, 1	295K
	conv4d	conv+bn+r	conv4c	3 × 3 × 128, 1, 1	147K
upblock2	upconv5a	tconv	conv4c	2, 2	32K
	concat5b	concat	upconv5a, conv2b	-	-
	conv5c	conv+bn+r	concat5b	3 × 3 × 64, 1, 1	73K
	conv5d	conv+bn+r	conv5c	3 × 3 × 64, 1, 1	37K
upblock3	upconv6a	tconv	conv5d	2, 2	66K
	concat6b	concat	upconv6a, conv1b	-	-
	conv6c	conv+bn+r	concat5b	3 × 3 × 256, 1, 1	664K
	conv6d	conv+bn+r	conv6c	3 × 3 × 256, 1, 1	590K
Segmentation Sub-Network	sega	conv+bn+r	conv6d	3 × 3 × 256, 1, 1	66K
	segb	conv	sega	1 × 1 × 2, 1, 0	0.5K
	lossce	loss	segb	Cross Entropy	-
Triplet Learning Sub-Network a	samph	samp-h	conv6d	hard negative	-
	lossh	loss	samph	Triplet Loss	-
Triplet Learning Sub-Network b	sampc	samp-c	conv6d	contour-aware	-
	lossc	loss	sampc	Triplet Loss	-
Triplet Learning Sub-Network c	sampr	samp-r	conv6d	random	-
	lossr	loss	sampr	Triplet Loss	-

calculation of distances among all triplets or even a mini-batch is computationally expensive. Therefore, the work in [18] proposed to use triplets that violate the triplet distance assumption.

Inspired by the focal loss proposed in [25], we assume that the hard negative samples can be revealed by the incorrect predictions. Under this assumption, we propose a focal hard negative triplet sampling strategy, which adopts the heatmap generated by the segmentation sub-network as the reference to find the negative anchors. Specifically, for each voxel, we first calculate the absolute difference between the prediction and its ground-truth label. Then, a threshold τ is applied to select the bad predictions with large differences as the hard samples. The operation can be written as:

$$s_{ij}^{hard} = \begin{cases} 1 & \text{if } |(\hat{y}_{ij} - y_{ij})| > \tau \\ 0 & \text{if } |(\hat{y}_{ij} - y_{ij})| \leq \tau \end{cases} \quad (1)$$

where $s_{ij}^{hard} = 1$ denotes that the pixel at point (i, j) is

labeled as a hard negative sample. The threshold τ in this work is set to 0.1. This means both the semi-hard (i.e., near threshold) samples and hard (i.e., far away from threshold) samples are used to construct the triplets. Finally, as shown in Fig. 5 (b), the intersection of hard sample map s and positive sample map p , i.e., the positive hard sample map, is used as anchors to generate the triplets.

iii) Contour-Aware Triplet Sampling: For organ (e.g., prostate and gland) segmentation in medical images, the organ boundaries are often clinically important, but hard to be distinguished. Moreover, FCNs are not capable to directly generate refined segmentation for blurry organ boundaries. Therefore, various works leverage the contour-aware strategy to enhance the boundary discriminate ability of FCN. Typically, the contour-aware strategy forces the network to give special focuses on the contours/boundaries of the target organ, by introducing either specific designed loss terms [26] or guidance [23], [27] to the network. Inspired

by the successes of these existing methods, we propose a special triplet sampling strategy to incorporate contour-awareness, i.e., the contour-aware triplet sampling, into voxel-triplet feature embedding. Specifically, in each training iteration, we randomly select a number of points located on the prostate boundary as anchors, and construct triplets via these contour-aware anchors (See in Fig. 5.(c)).

3.2.3 Multi-Task Learning

As the whole network is constructed of multiple branches with multiple guidance, we leverage the power of multi-task learning to train them simultaneously.

The triplet-based metric learning is performed after getting the hard-negative and contour-aware triplets. Given one triplet as $\{\xi_{k,l}, \xi_{i,j}, \xi_{m,n}\}$, we denote $\xi_{k,l}$ as the feature representation of the (k, l) th point (i.e., an anchor) on the feature map ξ . Similarly, $\xi_{i,j}$ is the feature representation of the (i, j) th point which has the same label as the anchor, while $\xi_{m,n}$ has the opposite label. The loss function $\mathcal{L}_{trip.}$ for voxel-triplet feature embedding is then defined as

$$\begin{aligned} \mathcal{L}_{trip.} = & \sum_{n=1}^N \sum_{k,l \in K} \sum_{i,j \in J} \sum_{m,n \in M} \underbrace{[\|\xi_{k,l} - \xi_{i,j}\|_2^2 - \|\xi_{k,l} - \xi_{m,n}\|_2^2 + \sigma]}_{\text{triplet loss}} \\ & + \beta \sum_{n=1}^N \sum_{k,l \in K} \sum_{i,j \in J} \underbrace{[\|\xi_{k,l} - \xi_{i,j}\|_2^2 + \epsilon]}_{\text{positive pair-wise loss}} \end{aligned} \quad (2)$$

where K denotes the anchor set, J denotes the voxel set of positive labels, M denotes the voxel set of negative labels. Specifically, $\mathcal{L}_{trip.}$ consists of two terms balanced by a hyper-parameter β . The first term is the conventional triplet loss term to control the distances between positive samples and negative samples. The second term is an intra-class loss term to control the cluster of the positive samples. The hyper-parameter σ denotes the margin to control the distance between positive pairs and negative pairs, and ϵ denotes the maximum distance of the positive pairs. In this paper, we set the hyper-parameters $\sigma = 0.7$, $\epsilon = 0.01$ and $\beta = 0.1$.

Concurrently, the segmentation sub-network is trained by minimizing the cross-entropy loss:

$$\mathcal{L}_{CE} = -\frac{1}{N} \sum_{n=1}^N \log(\hat{p}_n, l_n) \quad (3)$$

Considering that distance-based losses (e.g., triplet loss in Eq.(2)) are of large magnitude, we use a factor $\{\lambda = 0.01\}$ to balance these two kind of losses (i.e., cross-entropy loss and triplet loss). Therefore, the final loss can be formally written as,

$$\mathcal{L} = \mathcal{L}_{CE} + \lambda \sum_{t=1}^T \mathcal{L}_{trip} \quad (4)$$

where t denotes the t th triplet sampling strategy.

Notably, in the training phase, the network is optimized with two learning paths, i.e., the segmentation path and the triplet learning path. In the testing phase, the voxel-wise prediction is directly output by the segmentation path, without the voxel-triplet learning module.

4 EXPERIMENTAL RESULTS

4.1 Data Setup

We evaluate our method on a large planning CT image dataset containing 339 patient CT scans. The images were collected by North Carolina Cancer Hospital, and the prostate contours manually delineated by two clinicians are adopted as the ground-truth labels. The image size is $512 \times 512 \times (61 \sim 508)$, with in-plane resolution as $0.932 \sim 1.365\text{mm}$, and slice thickness as $1 \sim 3\text{mm}$. As the images were collected in a long period using different scanners, the image size and resolution are varied across the patients. Automatic segmentation on this dataset is challenging because: 1) the images include different patient positions and are of different sizes; 2) one patient only has one image in this planning image dataset. We randomly partition the dataset into 70% for training, 10% for validation and 20% for testing.

4.2 Implementation Details

Our method was implemented using the popular open-source framework *PyTorch* [28]. The training of the proposed network is accelerated by four NVidia GTX 1080Ti GPUs.

We only did necessary image pre-processing on the original CT scans. First, we used trilinear interpolation to normalize the image spacing into $1 \times 1 \times 1\text{mm}^3$. Then, to eliminate the influence caused by singular values, we normalized the image intensities to $[0, 255]$.

The images with body regions were cropped by a simple threshold-based method to reduce the black background noise. Then, a sliding window method was implemented on these cropped body image parts to generate 2-D training patches. In training, the patches were randomly cropped to have the size of $64 \times 64 \times 5$ in the first stage, and $64 \times 64 \times 3$ in the second stage. Please note that, we used multiple input slice channels to predict the label for the middle slice. In the testing phase, the predictions of the region images are directly obtained from the network. This strategy can better incorporate inter-slice context for 2-D based methods. To construct training data, we cropped 500 patches from each training image. In testing, we directly apply the trained network to the cropped and down-sampled body region images (in the first stage) or the organ region images (in the second stage) to avoid voting for the patch-wise predictions. The goal of the experiments is to verify the effectiveness of our proposed voxel-triplet feature embedding method in improving segmentation performance and therefore we deployed our model using 2-D architectures (instead of 3-D) to obtain viable and comparable results for all architectures is shorter amount of time.

The networks were trained with the batch size of 30 on each GPU. All the competitive networks were optimized by standard Stochastic Gradient Descent (SGD) algorithm. The learning rate was decayed from 0.01 by the 'Poly' decay method.

4.3 Metrics

We use four commonly used metrics to evaluate the performance of the proposed method: Dice Similarity Coefficient (DSC), Average Surface Distance (ASD), Positive Predict

TABLE 2
Different network configurations of the proposed TripletUNet (including conventional UNet as baseline).

Method	Sampling Strategy			Loss		
	Random	Hard Negative	Contour-Aware	Cross-Entropy	Positive Pair	Triplet
UNet (Baseline)	-	-	-	✓	-	-
TripletUNet-R-Sep	✓	-	-	✓	-	✓
TripletUNet-R	✓	-	-	✓	-	✓
TripletUNet-H	-	✓	-	✓	-	✓
TripletUNet-C	-	-	✓	✓	-	✓
TripletUNet-HR	✓	✓	-	✓	-	✓
TripletUNet-HC	-	✓	✓	✓	-	✓
TripletUNet-HP	-	✓	-	✓	✓	✓
TripletUNet-HRP	✓	✓	-	✓	✓	✓
TripletUNet-HCP	-	✓	✓	✓	✓	✓

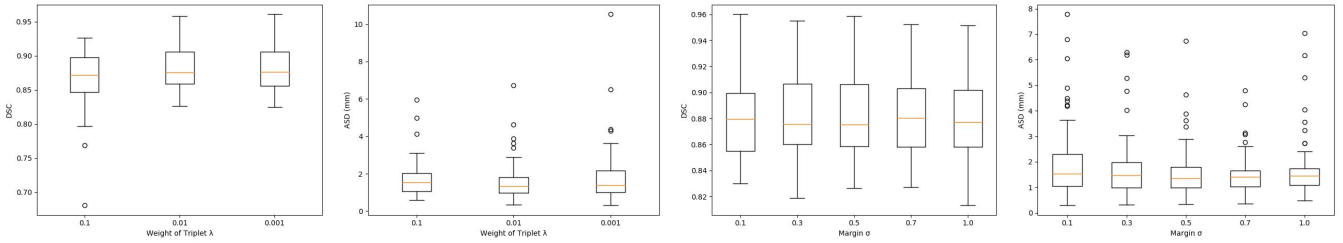


Fig. 6. The performance comparison in DSC and ASD of TripletUNet-R as a function of weight λ and margin σ .

Value (PPV) and Sensitivity (SEN). Let Vol_{seg} denote the volume of a prediction, Vol_{gt} denotes the volume of the ground-truth segmentation, and $d(a, b)$ denotes the Euclidean distance between point a and b . The four metrics can be written as,

(1) Dice Similarity Coefficient (DSC):

$$DSC = \frac{2\|Vol_{gt} \cap Vol_{seg}\|}{\|Vol_{gt}\| + \|Vol_{seg}\|}; \quad (5)$$

(2) Average Surface Distance (ASD):

$$ASD = \frac{1}{2} \left\{ \text{mean}_{a \in Vol_{gt}, b \in Vol_{seg}} \min d(a, b) + \text{mean}_{a \in Vol_{seg}, b \in Vol_{gt}} \min d(a, b) \right\}; \quad (6)$$

(3) Positive Predict Value (PPV) and Sensitivity (SEN):

$$PPV = \frac{\|Vol_{gt} \cap Vol_{seg}\|}{\|Vol_{seg}\|}; \quad SEN = \frac{\|Vol_{gt} \cap Vol_{seg}\|}{\|Vol_{gt}\|}. \quad (7)$$

4.4 Ablation Study

To analyze the importance of different components of our TripletFCN, we did comprehensive experiments to evaluate: 1) the effectiveness of triplet-based learning, and 2) the influence of different sampling strategies. Please note that, the aim of the ablation study is to verify the proposed triplet-based learning method. Therefore, for the convenience of perform the experiments, we use UNet as the backbone of TripletUNet. For the baseline method, we construct UNet to segment on the prostate region image which is same as the proposed two-stage learning framework. Obviously, using more recent variations of FCN (e.g., Res-UNet, VNet)

may achieve higher segmentation performance. For a fair comparison, we avoid using the advanced and complicated techniques for training of the deep networks, e.g., data augmentation, dropout, residual block, dense block, etc., for which can improve the segmentation performance of the network, with the aim to illustrate the effectiveness of the proposed triplet learning method. In this paper, we compose TripletUNets with six different configurations, with different combination of sampling strategies, architectures and losses. The setting of these networks in detail is listed in Table 2. The second set of row introduces the proposed networks trained by triplets from one sampling methods. The third set of row introduces the proposed networks trained by triplets from two sampling methods jointly. The suffix ‘Sep’ means the network is trained separately by the two losses, where the layer before the sampling layer is only trained under the guidance of triplet loss, and the layer after that is trained under the guidance of classification loss (i.e., the cross-entropy loss). We construct this network to evaluate the performance of pure-triplet learning.

4.4.1 The effectiveness of triplet-based learning

Firstly, we verified the effectiveness of the proposed triplet-based metric learning method from two aspects: 1) the converge rate, and 2) the segmentation accuracy.

The convergence analysis of the TripletUNet-R compared with the conventional UNet is illustrated in Fig. 7. Fig. 7 (a) and (b) show the cross-entropy loss and DSC curve of the two methods, respectively. The figure suggests that the incorporation of the proposed voxel-triplet learning module can boost the convergence of the segmentation network,

TABLE 3

Quantitative comparison of segmentation performance with TripletUNets in DSC, ASD(mm), SEN and PPV of different network configurations. All the networks are trained with the following hyper-parameters: $k = 20$, $m = 1$, $\sigma = 1.0$ and $\lambda = 0.01$.

Method	DSC		ASD		SEN		PPV	
	Mean \pm std	Median						
UNet (Baseline)	0.8376 \pm 0.0633	0.8501	3.8922 \pm 2.9335	2.9717	0.8733 \pm 0.0777	0.8819	0.8143 \pm 0.0918	0.8246
TripletUNet-R-Sep	0.8514 \pm 0.0506	0.8550	3.7606 \pm 2.7031	3.2781	0.8497 \pm 0.0829	0.8584	0.8616 \pm 0.0613	0.8717
TripletUNet-R	0.8817 \pm 0.0304	0.8784	1.4619 \pm 0.7715	1.2683	0.8727 \pm 0.0588	0.8700	0.8952 \pm 0.0449	0.9024
TripletUNet-H	0.8810 \pm 0.0302	0.8796	1.7695 \pm 1.1246	1.3915	0.8765 \pm 0.0582	0.8811	0.8897 \pm 0.0440	0.8940
TripletUNet-C	0.8822 \pm 0.0285	0.8775	1.6355 \pm 1.0693	1.2944	0.8732 \pm 0.0561	0.8697	0.8955 \pm 0.0437	0.8996
TripletUNet-HR	0.8822 \pm 0.0335	0.8776	1.4295 \pm 0.8719	1.2498	0.8760 \pm 0.0631	0.8777	0.8931 \pm 0.0444	0.8974
TripletUNet-HC	0.8804 \pm 0.0315	0.8750	1.3987 \pm 0.5836	1.2721	0.8714 \pm 0.0617	0.8768	0.8947 \pm 0.0475	0.8932
TripletUNet-HP	0.8811 \pm 0.0303	0.8790	1.5274 \pm 0.7687	1.3110	0.8719 \pm 0.0602	0.8694	0.8955 \pm 0.0474	0.8992
TripletUNet-HRP	0.8834 \pm 0.0302	0.8814	1.5701 \pm 0.9437	1.3329	0.8804 \pm 0.0592	0.8842	0.8907 \pm 0.0433	0.8953
TripletUNet-HCP	0.8839 \pm 0.0317	0.8828	1.3907 \pm 0.6651	1.2575	0.8805 \pm 0.0571	0.8798	0.8914 \pm 0.0452	0.8923

TABLE 4

Quantitative comparison of segmentation performance with TripletUNets with state-of-the-art methods. * denotes the results are reported on the 339 prostate dataset with the same data split.

Method	Type	Num. Cases	DSC	ASD	SEN	PPV
Costa <i>et al.</i> [29]	Deformable Model	16	-	-	0.75	0.80
Shao <i>et al.</i> [14]	Deformable Model + Random Forest	70	0.88 \pm 0.02	1.86 \pm 0.21	-	-
Gao <i>et al.</i> [15]	Deformable Model + Random Forest	313	0.87 \pm 0.04	1.77 \pm 0.66	0.88 \pm -	0.85 \pm -
Wang <i>et al.</i> [30]	Deep Learning	15	0.85 \pm 0.04	1.92 \pm 0.46	-	-
UNet <i>et al.</i> [3]*	Deep Learning + Two Stage	339	0.84 \pm 0.06	3.89 \pm 2.93	0.87 \pm 0.08	0.81 \pm 0.09
VNet <i>et al.</i> [4]*	Deep Learning + Two Stage	339	0.85 \pm 0.04	2.27 \pm 1.16	0.88 \pm 0.06	0.84 \pm 0.07
He <i>et al.</i> [23]*	Deep Learning + Two Stage	339	0.87 \pm 0.03	1.71 \pm 1.01	0.88 \pm 0.05	0.87 \pm 0.05
TripletUNet-HCP*	Deep Learning + Two Stage	339	0.88\pm0.03	1.39\pm0.66	0.88\pm0.05	0.89\pm0.04

since the network obtained more guidance from the pixel features.

The comparison of segmentation performance among different TripletUNets are reported in Table 3. It can be easily observed that, with the guidance of triplet learning, the performance of the network is significantly improved. The DSC of the TripletUNets reported in the first bar in Table 3 (i.e., TripletUNet-R,H,C) is improved by 4.41%, 4.34% and 4.46%, compared with baseline network UNet, which is trained by Cross-Entropy loss. Notably, in the proposed TripletUNets, we can observe that TripletUNet-R performs better among the three sampling methods. In DSC, TripletUNet-R method is slightly lower than TripletUNet-C; However, in ASD, TripletUNet-R outperform the TripletUNets with other two sampling methods by a margin. We conclude from the observation that random sampling can learn more integrated feature space in the proposed iteration based training scheme, since the other two sampling methods (i.e., focal hard negative sampling and contour-aware sampling) only sample from part of the whole feature space. The TripletUNet-HR and -HC networks, which are jointly learned on two sampling methods, both get a performance improvement on DSC and ASD, compared with TripletUNet-H and -C, which are only learned on one sampling methods. Moreover, as suggested by the table,

TripletUNet-HR did not perform better than TripletUNet-HC, which reveals the combination of two sampling methods can have the chance to learn more integrated feature space. Thus the advantage of using random sampling is indistinctive.

4.4.2 The influence of λ and σ

We compared the segmentation performance of TripletUNet-R in terms of different λ and σ to evaluate the influence of these two parameters. The networks were trained with the same settings of other hyper-parameters. We select several possible choices of the hyper-parameters as limited by time and computational resources. Fig. 6 shows the performance in DSC and ASD of TripletUNet-R with $\lambda \in \{0.1, 0.01, 0.001\}$. The figure indicates that choosing different σ may vary the performance of the proposed TripletUNet-R. As shown in the figure, the network performed best w.r.t. $\lambda = 0.01$. Fig. 6 also shows the performance in DSC and ASD of TripletUNet-R with $\sigma \in \{0.1, 0.3, 0.5, 0.7, 1.0\}$. It is suggested by the figure that the proposed network with $\sigma = 0.7$ performs best over other compared TripletUNets. The network achieves higher mean DSC and lower mean ASD. Moreover, the outliers in ASD are also closer to the mean ASD by this network compared with others.

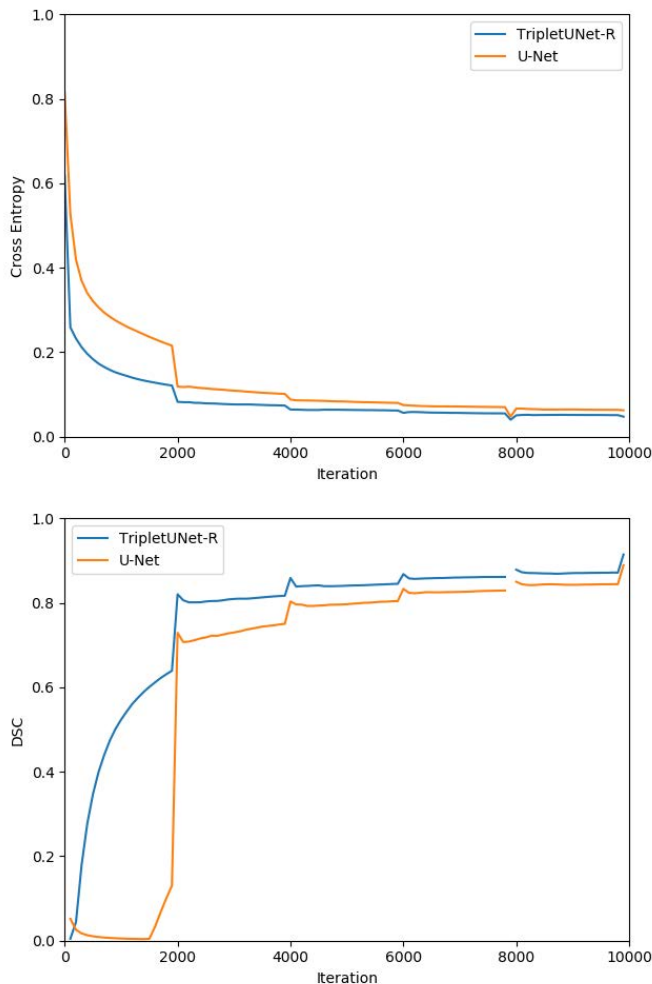


Fig. 7. The convergence analysis of UNet and the proposed TripletUNet-R.

4.5 Compare with the state-of-the-art methods

The quantitative comparison of the proposed TripletUNet with the state-of-the-art methods is reported in Table 4. We compare TripletUNet with several remarkable methods including deep learning-based methods and deformable model-based methods:

- Costa *et al.* [29] proposed a combination of deformable-model based method for the segmentation of prostate and bladder. The method is performed with different shape assumptions for the two organs.
- Shao *et al.* [14] introduced a deformable model-based segmentation method for prostate and rectum in CT images, where a local boundary regression method is performed on the near-organ regions.
- Gao *et al.* [15] proposed a deformable model-based segmentation method combined with a random forest to obtain the organ boundary. The initialization problem of deformable models is thus alleviated.
- Wang *et al.* [30] proposed a 3-D UNet based network with dilated convolution layers to improve the segmentation performance of prostate.

- Ronneberger *et al.* [3] proposed a fully convolutional network with two corresponding paths, namely UNet, with an encoding path and a decoding path with shortcut connections, so that the gradients in high-level can be better preserved to reach the low-level layers. The network is frequently used as the backbone and baseline in recent medical image segmentation studies.
- He *et al.* [23] proposed a two-stage UNet based network to segment the pelvic organs. Specifically, a novel morphological representation, namely distinctive curve, is incorporated to provide additional guidance for the network.
- Milletari *et al.* [4] proposed the VNet, in which a dice loss is proposed on a 3-D UNet based architecture with residual connections.

Obviously, the proposed method achieves the best overall segmentation performance among the listed methods. Among the compared methods, He *et al.*'s method in [23] outperform the other methods with a DSC value of 0.87 ± 0.03 and ASD value of 1.71 ± 1.01 . Compared with this method, our method obtains more than 1% improvement in DSC, from 0.87 to 0.88; and $0.32mm$ improvement in ASD, from 1.71 to 1.39, which is a 20% decreasing on the ASD value. The significant improvement on ASD indicates the effectiveness of the proposed method in delineating the organ contours, which is more valuable in clinical condition. Moreover, the proposed TripletUNet-HCP achieves 0.88 and 0.89 in mean SEN and PPV, respectively, which is significantly better than the deformable model-based method in [15] and the deep learning-based method in [23]. The tiny difference of the SEN and PPV value of the proposed method means that our proposed network is very robust at generating high quality segmentations, compared with the other methods. The robustness is also a key characteristic in clinical applications, where poor segmentation of the organ will lead to side effect. The conventional deep learning-based method in the second set of rows is not as good as the deformable models in the first set of rows. For example, VNet [4] achieves 0.85 ± 0.04 in DSC and 2.27 ± 1.16 in ASD, which is lower than the method in [15]. This can be because they were not specifically designed for the segmentation of prostate in CT images, which reveals the importance of incorporating domain knowledge and preserving the neighborhood information in the final segmentation map.

4.6 Visualization Results

We visualize the segmentation results of several typical cases generated by UNet, TripletUNet-H and TripletUNet-HCP in Fig. 8. As suggested by the figure, TripletUNet-HCP and TripletUNet-H can both generate more refined segmentations compare to the conventional UNet. Besides, TripletUNet-HCP performs better in some specific cases compared to TripletUNet-H. In very hard cases, over-segmentation or less-segmentation results are generated by UNet, while with triplet-based learning, TripletUNets often avoids these problems.

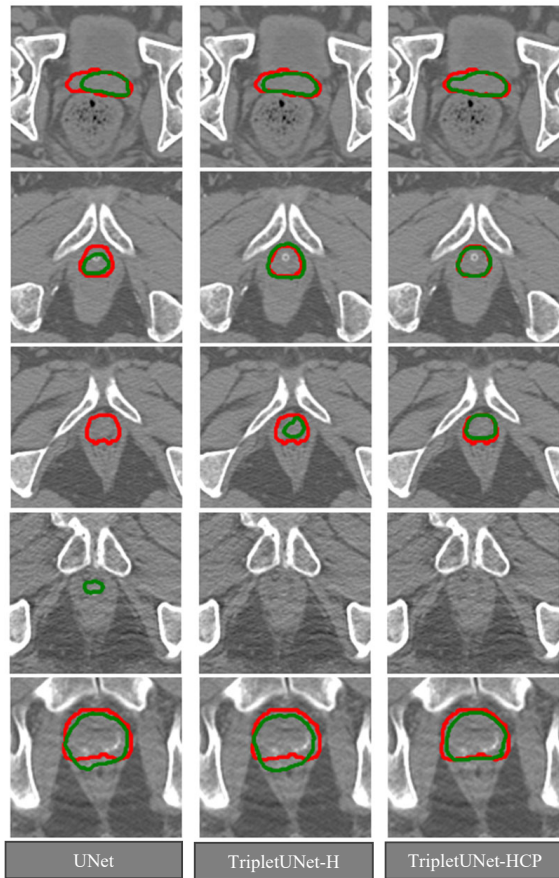


Fig. 8. The visualization of the results of UNet, TripletUNet-H and TripletUNet-HCP.

5 CONCLUSION

In this paper, we introduced a two-stage framework to accurately segment prostate from raw CT image. Specifically, in the first stage, the region of the prostate is quickly localized by a lightweight network with down-sampled CT image. In the second stage, a multi-task FCN guided by both segmentation information and voxel-level feature relationship is proposed for generating the fine segmentation map of prostate. The voxel-level feature relationship is learned by the proposed online voxel-triplet learning module.

Despite the effectiveness of the proposed triplet learning method, a more valuable contribution is that our voxel-triplet learning module suggests a promising direction of applying metric learning techniques into FCN-based pixel-to-pixel or voxel-to-voxel predictions. We conducted extensive experiments on a planning CT prostate image dataset, showing that the quality of deep features learned by FCN can be further improved by formulating the problem into a metric learning paradigm, without including any additional learnable parameters. Benefit by the generated voxel-level triplets, we can easily bring metric based weakly supervised learning and meta-learning methods into segmentation, which can be regarded as our future work.

Although the effectiveness of our method (i.e., TripletUNets) has been proved by the experiments, as a metric learning-based method, the computational efficiency of the proposed network should be further optimized. Naturally, how to boost the efficiency of metric learning method is still

an open question. Another intuitive question is to define more suitable metric learning methods for FCNs. Theoretically, the proposed voxel-triplet feature embedding module can be composed with every layer of the network, and thus reorder the features by learning with better designed metrics. These topics define direction for the future works.

REFERENCES

- [1] J. Long, E. Shelhamer, and T. Darrell, "Fully convolutional networks for semantic segmentation," in *Proceedings of the IEEE conference on computer vision and pattern recognition*, 2015, pp. 3431–3440.
- [2] J. Johnson, A. Karpathy, and L. Fei-Fei, "Densecap: Fully convolutional localization networks for dense captioning," in *Proceedings of the IEEE Conference on Computer Vision and Pattern Recognition*, 2016, pp. 4565–4574.
- [3] O. Ronneberger, P. Fischer, and T. Brox, "U-net: Convolutional networks for biomedical image segmentation," in *International Conference on Medical image computing and computer-assisted intervention*. Springer, 2015, pp. 234–241.
- [4] F. Milletari, N. Navab, and S.-A. Ahmadi, "V-net: Fully convolutional neural networks for volumetric medical image segmentation," in *2016 Fourth International Conference on 3D Vision (3DV)*. IEEE, 2016, pp. 565–571.
- [5] Ö. Çiçek, A. Abdulkadir, S. S. Lienkamp, T. Brox, and O. Ronneberger, "3d u-net: learning dense volumetric segmentation from sparse annotation," in *International conference on medical image computing and computer-assisted intervention*. Springer, 2016, pp. 424–432.
- [6] C. Lian, J. Zhang, M. Liu, X. Zong, S.-C. Hung, W. Lin, and D. Shen, "Multi-channel multi-scale fully convolutional network for 3d perivascular spaces segmentation in 7t mr images," *Medical image analysis*, vol. 46, pp. 106–117, 2018.
- [7] J. Dai, Y. Li, K. He, and J. Sun, "R-fcn: Object detection via region-based fully convolutional networks," in *Advances in neural information processing systems*, 2016, pp. 379–387.
- [8] L. Bertinetto, J. Valmadre, J. F. Henriques, A. Vedaldi, and P. H. Torr, "Fully-convolutional siamese networks for object tracking," in *European conference on computer vision*. Springer, 2016, pp. 850–865.
- [9] C. Lian, M. Liu, J. Zhang, and D. Shen, "Hierarchical fully convolutional network for joint atrophy localization and alzheimer's disease diagnosis using structural mri," *IEEE transactions on pattern analysis and machine intelligence*, 2018.
- [10] L. Chen, G. Papandreou, I. Kokkinos, K. Murphy, and A. L. Yuille, "DeepLab: Semantic image segmentation with deep convolutional nets, atrous convolution, and fully connected crfs," *IEEE Trans. Pattern Anal. Mach. Intell.*, vol. 40, no. 4, pp. 834–848, 2018. [Online]. Available: <https://doi.org/10.1109/TPAMI.2017.2699184>
- [11] R. Trullo, C. Petitjean, S. Ruan, B. Dubray, D. Nie, and D. Shen, "Segmentation of organs at risk in thoracic ct images using a sharpmask architecture and conditional random fields," in *2017 IEEE 14th International Symposium on Biomedical Imaging (ISBI 2017)*. IEEE, 2017, pp. 1003–1006.
- [12] D. Cheng, Y. Gong, S. Zhou, J. Wang, and N. Zheng, "Person re-identification by multi-channel parts-based cnn with improved triplet loss function," in *Proceedings of the IEEE Conference on Computer Vision and Pattern Recognition*, 2016, pp. 1335–1344.
- [13] O. M. Parkhi, A. Vedaldi, A. Zisserman *et al.*, "Deep face recognition," in *bmvc*, vol. 1, no. 3, 2015, p. 6.
- [14] Y. Shao, Y. Gao, Q. Wang, X. Yang, and D. Shen, "Locally-constrained boundary regression for segmentation of prostate and rectum in the planning ct images," *Medical image analysis*, vol. 26, no. 1, pp. 345–356, 2015.
- [15] Y. Gao, Y. Shao, J. Lian, A. Z. Wang, R. C. Chen, and D. Shen, "Accurate segmentation of ct male pelvic organs via regression-based deformable models and multi-task random forests," *IEEE Transactions on Medical Imaging*, vol. 35, no. 6, pp. 1532–1543, 2016.
- [16] Y. Shi, Y. Gao, S. Liao, D. Zhang, Y. Gao, and D. Shen, "Semi-automatic segmentation of prostate in ct images via coupled feature representation and spatial-constrained transductive lasso," *IEEE transactions on pattern analysis and machine intelligence*, vol. 37, no. 11, pp. 2286–2303, 2015.

- [17] Y. Shi, W. Yang, Y. Gao, and D. Shen, "Does manual delineation only provide the side information in ct prostate segmentation?" in *International Conference on Medical Image Computing and Computer-Assisted Intervention*. Springer, 2017, pp. 692–700.
- [18] F. Schroff, D. Kalenichenko, and J. Philbin, "Facenet: A unified embedding for face recognition and clustering," in *Proceedings of the IEEE conference on computer vision and pattern recognition*, 2015, pp. 815–823.
- [19] W. Liu, Y. Wen, Z. Yu, M. Li, B. Raj, and L. Song, "Sphereface: Deep hypersphere embedding for face recognition," in *Proceedings of the IEEE conference on computer vision and pattern recognition*, 2017, pp. 212–220.
- [20] S. Ding, L. Lin, G. Wang, and H. Chao, "Deep feature learning with relative distance comparison for person re-identification," *Pattern Recognition*, vol. 48, no. 10, pp. 2993–3003, 2015.
- [21] F. Wang, W. Zuo, L. Lin, D. Zhang, and L. Zhang, "Joint learning of single-image and cross-image representations for person re-identification," in *Proceedings of the IEEE Conference on Computer Vision and Pattern Recognition*, 2016, pp. 1288–1296.
- [22] L. A. Lim and H. Y. Keles, "Foreground segmentation using a triplet convolutional neural network for multiscale feature encoding," *arXiv preprint arXiv:1801.02225*, 2018.
- [23] K. He, X. Cao, Y. Shi, D. Nie, Y. Gao, and D. Shen, "Pelvic organ segmentation using distinctive curve guided fully convolutional networks," *IEEE transactions on medical imaging*, vol. 38, no. 2, pp. 585–595, 2019.
- [24] Y. Duan, W. Zheng, X. Lin, J. Lu, and J. Zhou, "Deep adversarial metric learning," in *Proceedings of the IEEE Conference on Computer Vision and Pattern Recognition*, 2018, pp. 2780–2789.
- [25] T.-Y. Lin, P. Goyal, R. Girshick, K. He, and P. Dollár, "Focal loss for dense object detection," in *Proceedings of the IEEE international conference on computer vision*, 2017, pp. 2980–2988.
- [26] Y. Zhou, O. F. Onder, Q. Dou, E. Tsougenis, H. Chen, and P.-A. Heng, "Cia-net: Robust nuclei instance segmentation with contour-aware information aggregation," *arXiv preprint arXiv:1903.05358*, 2019.
- [27] H. Chen, X. Qi, L. Yu, Q. Dou, J. Qin, and P. Heng, "DCAN: deep contour-aware networks for object instance segmentation from histology images," *Medical Image Analysis*, vol. 36, pp. 135–146, 2017. [Online]. Available: <https://doi.org/10.1016/j.media.2016.11.004>
- [28] A. Paszke, S. Gross, S. Chintala, G. Chanan, E. Yang, Z. DeVito, Z. Lin, A. Desmaison, L. Antiga, and A. Lerer, "Automatic differentiation in pytorch," in *NIPS-W*, 2017.
- [29] M. J. Costa, H. Delingette, S. Novellas, and N. Ayache, "Automatic segmentation of bladder and prostate using coupled 3d deformable models," in *International Conference on Medical Image Computing and Computer-Assisted Intervention*. Springer, 2007, pp. 252–260.
- [30] B. Wang, Y. Lei, T. Wang, X. Dong, S. Tian, X. Jiang, A. B. Jani, T. Liu, W. J. Curran, P. Patel *et al.*, "Automated prostate segmentation of volumetric ct images using 3d deeply supervised dilated fcn," in *Medical Imaging 2019: Image Processing*, vol. 10949. International Society for Optics and Photonics, 2019, p. 109492S.